

Quantum Advantage for All

CHRISTOPH M. KIRSCH, University of Salzburg, Austria and Czech Technical University, Prague, Czech Republic
STEFANIE MUROYA LEI, Czech Technical University, Prague, Czech Republic

We show how to translate a subset of RISC-V machine code compiled from a subset of C to quadratic unconstrained binary optimization (QUBO) models that can be solved by a quantum annealing machine: given a bound n , there is input I to a program P such that P runs into a given program state E executing no more than n machine instructions if and only if the QUBO model of P for n evaluates to 0 on I . Thus, with more qubits on the machine than variables in the QUBO model, quantum annealing the model reaches 0 (ground) energy in constant time with high probability on some input I that is part of the ground state if and only if P runs into E on I executing no more than n instructions. Translation takes $O(n^2)$ time effectively turning a quantum annealer into a *polynomial-time symbolic execution engine and bounded model checker*, eliminating their path and state explosion problems. Here, we take advantage of the fact that any machine instruction may only increase the size of the program state by a constant amount of bits. Translation time comes down from $O(n^2)$ to $O(n \cdot |P|)$ if memory consumption of P is bounded by a constant, establishing a linear (quadratic) upper bound on quantum space, in number of qubits on a quantum annealer, in terms of algorithmic time (space) in classical computing, implying $NP \subseteq BQP$. Our prototypical open-source toolchain¹ translates machine code that runs on real RISC-V hardware to models that can be solved by real quantum annealing hardware², as shown in our experiments.

Additional Key Words and Phrases: symbolic execution, bounded model checking, quantum annealing

1 INTRODUCTION AND OVERVIEW

Unlike universal quantum computers, quantum annealers can essentially only solve optimization problems but tend to have a lot more qubits and are much easier to program because of their relative simplicity. On a quantum annealer, each qubit has a programmable bias towards 0 or 1, expressed as linear factor of a binary variable x that represents the qubit in a quadratic unconstrained binary optimization (QUBO) model. Moreover, each qubit can be quantitatively entangled with any other qubit, at least logically, expressed as bi-linear³ factor of two variables x and y that represent the entangled qubits in the QUBO model. The terms (binary) variable and qubit are therefore logically synonymous. Once bias and entanglement are configured as linear and bi-linear factors, quantum annealing refers to the constant-time process of moving from a high energy state in which all qubits are in superposition to a low (ground) energy state in which all qubits are 0 or 1 and represent a solution of the QUBO model with some probability that can be increased by repeating the process and tuning the model. In short comedic terms, quantum annealing is like a shaman throwing bones except that some physical properties of the bones are programmable. On a more serious note, we discuss work related to quantum annealing in Section 2 right after the introduction.

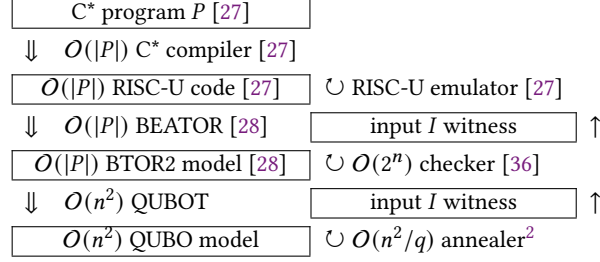
Fig. 1 provides an overview of the selfie toolchain¹ that we developed for symbolic execution [12, 26] and bounded model checking [8] in linear (quadratic) time on quantum annealers. The C* compiler is a non-optimizing linear-time compiler from a tiny subset of C called C* to a tiny subset of 64-bit RISC-V called RISC-U, supporting only unsigned integer arithmetic. BEATOR [28] translates in linear time RISC-U code to a model in a subset of BTOR2 [36] that is input to bounded model checkers such as btor mc [36]. Compilation and translation guarantee: there is input I to a C* program P for which the compiled RISC-U code of P runs into an error state E such as division by zero after executing

¹<https://github.com/cksystemsteaching/selfie/tree/quantum>

²www.dwavesys.com

³an example of a bi-linear factor is $-2xy$ whereas a quadratic factor such as $-2x^2$ is a linear factor if x is a binary variable because then $-2x^2 = -2x$

Authors' addresses: Christoph M. Kirsch, University of Salzburg, Austria and Czech Technical University, Prague, Czech Republic, ck@cs.uni-salzburg.at; Stefanie Muroya Lei, Czech Technical University, Prague, Czech Republic, stefanie.muroya@ucsp.edu.pe.

Fig. 1. Selfie toolchain¹ and workflow

n RISC-U instructions if and only if E is reachable on I in $O(n)$ state transitions in the BTOR2 model of P . An input I found by a bounded model checker may then be validated as witness of E by running the RISC-U code on I to see if E is indeed triggered. The key idea of the translation is to model the full machine state (program counter, registers, memory) as state variables and then update them via two combinational circuits generated from the control and data flow of the code. The toolchain from C* via RISC-U to BTOR2 is written in C* in around 15-KLOC [1, 2, 27, 28]. We enhanced BEATOR in around 1.5-KLOC with support of a down-scaled linear address space, a segmenting MMU and RAM model, dead code elimination, constant propagation, and 32-bit machines and code (the rest of the toolchain already had 32-bit support), see Section 3.

QUBOT is new, written in Python in around 3-KLOC, and our main technical contribution, besides the enhancements to BEATOR. Given a C* program P and a bound n , it translates in $O(n^2)$ time the BTOR2 model B of P to a QUBO model such that there is input I on which an error state E is reachable in no more than n state transitions in B if and only if the QUBO model evaluates to 0 on I . Thus, with more qubits on the machine than variables in the QUBO model, quantum annealing the model reaches 0 (ground) energy in constant time with high probability on some input I that is part of the ground state if and only if E is reachable on I in no more than n state transitions in B . Similar to classical bounded model checkers, quantum annealing may only be able to determine some but not all such inputs efficiently. However, known inputs help debugging QUBOT by enabling validation of QUBO models even without any quantum annealing: a generated QUBO model must evaluate to 0 (ground energy) on any input that leads to an error in no more than n state transitions in the original BTOR2 model, and otherwise evaluate to a value greater than 0 (high energy).

The key challenge in the translation is to encode reachability in a state machine (BTOR2 model) in a stateless binary quadratic function (QUBO model). The key idea of QUBOT is to model the input I and state variables S in a BTOR2 model in $O(n)$ qubits (binary variables) that are biased and entangled with another set of $O(n)$ qubits that represent the output of the combinational circuits for control and data flow on I and S [37]. Here, we take advantage of the fact that any machine instruction may only increase the size of the program state by a constant amount of bits. At least logically, we then duplicate the model n times where, for all $0 \leq i < n$, duplicate D_i is entangled with duplicate D_{i+1} such that each qubit o in D_i that represents an output of a combinational circuit in the BTOR2 model is used in D_{i+1} as qubit that represents the part of the state variable in the BTOR2 model which o updates [37]. Input variables are introduced in each duplicate as uninitialized state variables. QUBOT propagates constants and initial values of state variables at bit level (not word level) for reducing the number of qubits.

The superposition of all qubits in a duplicate D_i represents all possible control- and data-flow paths through the code after executing $O(i)$ instructions. Quantum annealing of the QUBO model takes constant time if the number of qubits q available on the quantum annealer is greater than the number of variables in the model. Otherwise, annealing may work

in $O(n^2/q)$ time using a hybrid solver [30]. The size of the model comes down to $O(n \cdot |P|)$ if memory consumption of P is bounded by a constant. The input found through quantum annealing may again be validated as witness of the error similar to witnesses found through classical bounded model checking. All the details are in Section 4.

While going through the toolchain from C* via RISC-U to BTOR2 takes time and effort, there are important qualitative and quantitative reasons to do so. Firstly, the toolchain motivates, explains, and enables the design of our bounded model checker on a quantum annealer with an immediate connection back to real code. Secondly, we enhanced BEATOR significantly providing important insight into the tradeoff between BEATOR's and QUBOT's complexity and to enable our experiments. Thirdly, and most importantly, the full selfie toolchain establishes the main principled contribution of this paper: a linear (quadratic) upper bound on quantum space, in number of qubits on a quantum annealer, in terms of algorithmic time (space) in classical computing, implying $NP \subseteq BQP$.

That result motivates *evidential programming* for quantum annealers: generate code that merely checks whether its input is evidence of a solution to a given problem instance and then use a toolchain as presented here and a quantum annealer as oracle to compute the input [37]. For example, think of implementing a linear-time SAT solver by generating code for a given SAT formula that checks whether a variable assignment satisfies the formula. In other words, that programming paradigm makes quantum annealers superpolynomial accelerators in classical computing far beyond what GPUs and other constant-factor accelerators can do.

This does not mean, of course, that NP is suddenly equal to P. However, bounded quantum space suggests that *quantum advantage*, rather than being a property of quantum hardware when solving *hard* problems, is actually a property of classical software for solving *any* problem where we either run out of classical time before we run out of quantum space, or vice versa, motivating a *metric* as defined in Section 4.1: the less classical time and the more quantum space, the more quantum advantage you have, and vice versa. In fact, with that metric, we can even predict, for any given classical software, how many qubits it takes until gaining quantum advantage.

Quantum engineers hopefully keep building quantum annealers with more and more qubits, but, just like decades ago in classical computing, there is also a large-scale community effort waiting to happen to invent the necessary languages, tools, and runtimes that, this time, bring down the need for qubits. In short, any lower bound on qubits may be equal to the upper bound we present here but there is still a lot of room for large constant-factor improvements and, with some luck, even more than that. As an example, we speculate about a universal quantum computer based on what we call a *quantum advantage processing unit* (QAPU) which could indeed lower the quadratic upper bound on qubits to linear and even constant space, see Section 4.2. Another important issue is to determine whether QUBO is the correct abstraction for isolating us from physics, similar to Boolean algebra in classical computing, see the conclusions in Section 6 for more.

Nevertheless, what may seem disappointing for now but hardly comes as surprise is the fact that the qubit capacity of currently available quantum annealers is still quite limited making it hard (but not impossible) to anneal even our simple running example introduced in Section 3. We only managed to do it anyway by optimizing BEATOR and QUBOT. Another issue is that qubits on existing quantum annealers cannot be entangled with all other qubits. Thus annealing QUBO models in practice requires solving an optimization problem called *minor embedding* which is NP-hard itself. In other words, the upper bounds on translation time presented here only apply, either to ideal quantum annealers where all qubits can be entangled with all other qubits, or else to any quantum annealer by assuming that minor embeddings can be found in linear time using, well, a quantum annealer, where finding those minor embeddings must not involve the selfie toolchain when bootstrapping selfie. That being said minor embeddings can be solved efficiently and sufficiently accurate using heuristics. The following section and Section 5 on experiments have more on that.

2 RELATED WORK

We found inspiration from two, separate lines of thought that we bring together here: (1) translation of classical code to quantum annealers [24, 37] and (2) symbolic execution [26], from systems such as KLEE [12] and S2E [13], and from bounded model checking [8], such as the bounded model checker btormc [36]. Satisfiability Modulo Theory (SMT) solvers such as Z3 [17] and boolector [35], and the fact that SAT and SMT formulae can be solved using quantum annealers have helped us as well [7, 10, 18, 42, 49].

While BEATOR and QUBOT together logically resemble translation of Verilog to QMASM via EDIF [37], there are a number of technical advancements as well as an important principled difference: firstly, our toolchain translates *any* 64-bit C* code, in particular C* code using dynamic memory, and not Verilog [37] or domain-specific C code targeting quantum annealers [24]. Secondly, unlike [37], it supports symbolic execution and bounded model checking not just on the theory of bitvectors but, most importantly, on the theory of arrays of bitvectors as well which is key to supporting dynamic memory allocation. Thirdly, it enables relating classical algorithmic complexity with spatial quantum complexity by lifting translation of classical code [37] to symbolic execution and bounded model checking on quantum annealers. However, our toolchain currently defers handling minor embeddings to a D-Wave library² at the expense of improved annealing performance [37].

BTOR2 [36] extends SMT-LIB [4] with sequential operators enabling us to avoid the path explosion problem in symbolic execution engines. Translating BTOR2 to quadratic unconstrained binary optimization (QUBO) models takes us to the domain of QUBO problems and solvers. QUBO is NP-hard [16] and has numerous applications beyond quantum annealing [29]. QUBO problems can be solved by Steepest Gradient Descent [33] and Tabu Search [20] as well as variations of Tabu Search [6, 21, 34, 38, 51], Simulated Quantum Annealing (SQA) [14, 46], and Global Equilibrium Search (GES) [40, 41]. SQA algorithms use Markov Chain Monte Carlo methods [14] and classical accelerators such as GPUs and FPGAs [46] to deal with the problem that current quantum computers feature only relatively small amounts of qubits. Optimization techniques found in QUBO solvers but also SMT solvers and bounded model checkers as well as in compilers may eventually help reducing the number of qubits when translating RISC-V via BTOR2 to QUBO.

Moving on to quantum computing, there are essentially two mainstream models of quantum computers or Noisy Intermediate-Scale Quantum (NISQ) devices: gate model (GM) and quantum annealing (QA) machines. Our results apply to QA, not GM. While GM is universal, QA is not. However, in the NISQ-devices market [15], QA greatly outperforms GM in number of available qubits with the most recently released Quantum Processor Unit (QPU) featuring 5k qubits, and the announcement of a QPU with 7k qubits. Moreover, QA has recently been shown to return global optima with higher probability than GM while both, QA and GM, do not provide fairness if multiple ground states exist [39]. QA has already been applied in various domains other than executing arbitrary code [3, 32, 43, 45, 47].

In principle, QA can solve any QUBO model. However, for QA to work QUBO models still need to be minor-embedded onto the particular architecture of a machine where not all qubits can be entangled with all other qubits. Finding proper minor embeddings [5, 11, 16, 50] is an NP-hard problem itself and important to enable quantum annealing and increase performance [37]. Improving the QUBO models to enhance the solution space [31, 44], considering how various parameters in the annealing process affect results [22, 25], and addressing the problem of too many binary variables versus too few available qubits [30] is important as well.

```

uint64_t* x;
uint64_t main() { uint64_t a;
  x = malloc(1); // rounded up to 8
  // touch to trigger page fault here
  *x = 0;
  // read 1 byte from console into x
  read(0, x, 1);
  // copy from heap to stack segment
  a = *x;
  // decrement input until <= '0'
  while (a > '0')
    a = a - 1;
  // segmentation fault on input '1'
  if (a == *x - 1) // '0' == '1' - 1
    // segfault: '0' != 0
    a = *(x + a);
  return 0;
}

```

Fig. 2. Running example of a C* program

3 CLASSICAL MODELING WITH BEATOR

We introduce, by running example, the previously published part of the selfie toolchain [1, 2, 27, 28] that provides the foundation of our work here and is available as open source¹. We have also added new features to the toolchain that enable us trading off translation complexity between BEATOR and QUBOT. Those are mentioned below.

3.1 C* [27]

Consider the source code of the running example in Fig. 2. The program reads a single byte from the console keyboard and returns zero as exit code unless the user presses 1 in which case a segmentation fault may be triggered by the attempt to read from unallocated memory with $*(x + a)$ since a is then `'0'` which is 48, and not 0. Below we consider certain types of unsafe memory access triggering segmentation faults as well as non-zero exit codes and division by zero as error states. The toolchain is able to compute program input that leads to such error states. Program input is all read input. Once some input has been determined the code can be executed on that input to validate if an error state is actually reached.

The code is written in C* which is a tiny subset of C that has originally been developed for educational purposes. The example essentially features all elements of C* except procedure calls. C* only features two data types, `uint64_t` and `uint64_t*`, and five statements: assignment, while, if, return, and procedure call. There are the usual arithmetic and comparison operators but only for unsigned 64-bit integer arithmetic. Notably, there is only the unary dereference operator `*` to access heap memory. There are no arrays and no structs hence the name C*. Furthermore, C* supports integer, character, and string literals as well as global and local variables and procedure parameters. Lastly, there is `printf` library support and a total of five builtin procedures: `exit`, `open`, `read`, `write`, and `malloc`. Turns out that, because of its overall simplicity and in particular its focus on unsigned integer arithmetic, C* is well-suited as target for researching and prototyping tools for symbolic execution [12, 17, 26, 36].

The part of the toolchain that is relevant here is written in C* and consists of a non-optimizing C* compiler that targets RISC-U, a tiny subset of 64-bit RISC-V [48], as well as a RISC-U emulator and BEATOR which translates RISC-U

```

WHILE: ld t0, -8(s0)      // t0=a
      addi t1, zero, 48  // t1='0'
      sltu t0, t1, t0    // t0='0'<a
      beq t0, zero, 6[IF] // goto IF '0'=>a
      ld t0, -8(s0)      // t0=a
      addi t1, zero, 1   // t1=1
      sub t0, t0, t1      // t0=a-1
      sd t0, -8(s0)      // a=a-1
      jal zero, -8[WHILE] // goto WHILE
IF:   ld t0, -8(s0)      // t0=a
      ld t1, -16(gp)     // t1=x
      ld t1, 0(t1)       // t1=*x
      addi t2, zero, 1   // t2=1
      sub t1, t1, t2      // t1=*x-1
      sub t0, t1, t0      // t0=*x-1-a
      addi t1, zero, 1   // t1=1
      sltu t0, t0, t1     // t0=*x-1-a<1
      beq t0, zero, 8[R0] // goto R0 *x-1!=a
A0:   ld t0, -16(gp)     // t0=x
      ld t1, -8(s0)      // t1=a
      addi t2, zero, 8   // t2=8 (bytes)
      mul t1, t1, t2      // t1=a*8
A1:   add t0, t0, t1      // t0=x+a*8
SEGFL: ld t0, 0(t0)      // t0=*(x+a)
      sd t0, -8(s0)      // a=*(x+a)
R0:   addi t0, zero, 0    // t0=0
      addi a0, t0, 0      // a0=0
      jal zero, 1[EXIT]  // return 0 (a0)

```

Fig. 3. RISC-U assembly fragment generated for the running example in Fig. 2

code to BTOR2 [36]. RISC-U binaries generated by the C* compiler are in ELF format and run not only on the RISC-U emulator but also on QEMU and actual 64-bit RISC-V hardware. The toolchain also fully supports 32-bit machines and generates 32-bit code by bootstrapping `uint64_t` to `uint32_t` and carefully avoiding integer overflows beyond 32 bits. Only BEATOR used to be limited to 64-bit binaries. We have added 32-bit support to BEATOR to highlight the impact of machine word size on number of qubits in Section 5. Thus everything below also applies to 32-bit machines and code.

3.2 RISC-U ISA [27, 48]

Consider the RISC-U assembly fragment in Fig. 3 which has been generated by the C* compiler for the while loop as well as the if and the return statements in the running example. The assembly fragment features 9 out of the 14 RISC-U instructions. Overall code size is linear in the size of the C* source. Labels and comments are provided manually.

In order to familiarize yourself with the instruction set, consider Table 1 which shows syntax and semantics of the 14 RISC-U instructions. Similar to C*, RISC-U only supports unsigned 64-bit integer arithmetic, hence the name RISC-U.

A RISC-U machine has a 64-bit program counter denoted `pc`, 32 general-purpose 64-bit registers numbered 0 to 31 and denoted `zero`, `ra`, `sp`, `gp`, `tp`, `t0-t2`, `s0-s1`, `a0-a7`, `s2-s11`, `t3-t6`, and 4GB of byte-addressed main memory. Register `zero` always contains the constant value 0. RISC-U binaries only use up to 18 of the 32 general-purpose

Initialization	
lui rd,imm	$rd \leftarrow imm * 2^{12}; pc \leftarrow pc + 4$
addi rd,rs1,imm	$rd \leftarrow rs1 + imm; pc \leftarrow pc + 4$
Memory	
ld rd,imm(rs1)	$rd \leftarrow mem[rs1 + imm]; pc \leftarrow pc + 4$
sd rs2,imm(rs1)	$mem[rs1 + imm] \leftarrow rs2; pc \leftarrow pc + 4$
Arithmetic	
add rd,rs1,rs2	$rd \leftarrow rs1 + rs2; pc \leftarrow pc + 4$
sub rd,rs1,rs2	$rd \leftarrow rs1 - rs2; pc \leftarrow pc + 4$
mul rd,rs1,rs2	$rd \leftarrow rs1 * rs2; pc \leftarrow pc + 4$
divu rd,rs1,rs2	$rd \leftarrow rs1 /_{unsigned} rs2; pc \leftarrow pc + 4$
remu rd,rs1,rs2	$rd \leftarrow rs1 \%_{unsigned} rs2; pc \leftarrow pc + 4$
Comparison	
sltu rd,rs1,rs2	$rd \leftarrow \begin{cases} 1, & \text{if } rs1 <_{unsigned} rs2 \\ 0, & \text{otherwise} \end{cases}$ $pc \leftarrow pc + 4$
Control	
beq rs1,rs2,imm	$pc \leftarrow \begin{cases} pc + imm, & \text{if } rs1 == rs2 \\ pc + 4, & \text{otherwise} \end{cases}$
jal rd,imm	$rd \leftarrow pc + 4; pc \leftarrow pc + imm$
jalr rd,imm(rs1)	$tmp \leftarrow ((rs1 + imm) /_{unsigned} 2) * 2;$ $rd \leftarrow pc + 4; pc \leftarrow tmp$
System	
ecall	system call number in a7, parameters in a0–a3, return value in a0

Table 1. Table of the 14 RISC-U instructions [27]

registers, namely zero, ra which stands for *return address*, sp for *stack pointer*, gp for *global pointer*, t0–t6 where the t stands for *temporary*, s0 where the s stands for *saved*, and a0–a3 and a6–a7 where a stands for *argument*.

RISC-U instructions are encoded in 32 bits (4 bytes) each and stored next to each other in memory such that there are two instructions per 64-bit double word. Memory, however, can only be accessed at 64-bit double-word granularity. The d in ld and sd stands for double word. Below we nevertheless refer to double word by machine or memory word or just word for brevity. The parameters rd, rs1, and rs2 denote any of the general-purpose registers. The parameter imm denotes an *immediate* value which is a signed integer in two's complement represented by a fixed number of bits depending on the instruction. The five builtin procedures of C* are implemented by five system calls that follow the ABI of Linux and the official RISC-V toolchain enabling RISC-U binaries to run on both platforms as well.

The RISC-U memory layout is shown in Fig. 4. Code starts by RISC-V convention at 0x10000 and ends for our running example at 0x10228. The data segment starts 4KB-page-aligned after the code segment at 0x11000 and ends at 0x11010, again for our running example. The data segment contains values of global variables, string literals, and big integer literals that require more than 32 bits up to 64 bits. The layout of the data segment does not change during code execution. Entries are addressed relative to register gp which is initialized by the executed code, here to 0x11010, and then never changed. In our running example, the data segment contains two 64-bit memory words, one for the global variable x at gp-16 and one for an internal variable _bump at gp-8 which facilitates a bump-pointer allocator for malloc. The _bump pointer is initialized by the executed code to the start of the heap which is 4KB-page-aligned after

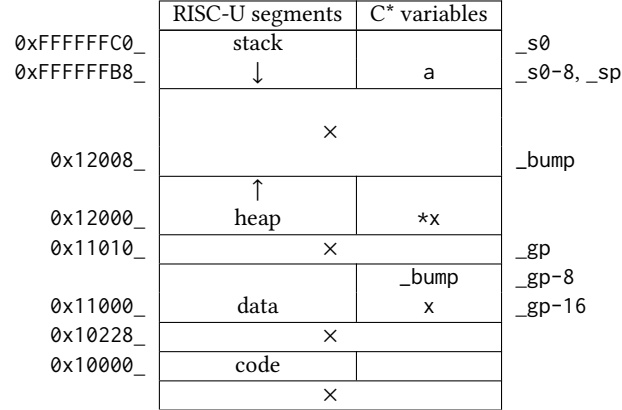


Fig. 4. 4KB-page-aligned RISC-U memory segments and machine state when executing the RISC-U code in Fig. 3

the end of the data segment, here at 0x12000. After executing `x = malloc(1);`, the `_bump` pointer is increased by 8 bytes (64 bits), rounded up from 1 byte, to 0x12008. The allocated address returned by `malloc` is the previous value of `_bump` which is 0x12000, hence making `x` point to the first 64-bit memory word `*x` on the heap. The byte read from the console keyboard by the `read(0, x, 1)` call is stored in the least significant byte of that memory word with the more significant bytes set to 0.

The stack segment starts at the address where register `sp` points to, here 0xFFFFFB8, which is the top of the call stack. The end of the stack segment is the highest address in main memory. Thus the call stack grows downwards to lower addresses while the heap grows upwards to higher addresses towards the stack. There is currently no free call in the system but it could be added without affecting modeling. The call stack and register `sp` are initialized by the boot loader. Local variables and procedure parameters on the call stack are accessed relative to register `s0` called the *frame pointer*. Here, the local variable `a` is at the top of the stack at `s0-8` where `s0` is set to 0xFFFFFC0 by the callee of the currently executed procedure, that is, here the main procedure.

In sum, the state of a RISC-U machine consists of the 64-bit program counter, the 18 general-purpose 64-bit registers, and the 64-bit memory words in the data, heap, and stack segments. Both, BEATOR and QUBOT must handle that state.

3.3 BTOR2 [36] (BEATOR2 [28])

BTOR2 is a formalism [36] for modeling finite state machines over the theory of bitvectors and arrays of bitvectors. Essentially, BTOR2 extends the bitvector fragment of SMT-LIB [4] with sequential operators for states and state transitions. BTOR2 models are input to bounded model checkers [8] such as `btormc` [36]. Given a BTOR2 model, a bounded model checker determines whether there is input to the model such that it transitions from its initial state to a bad state in a given number of state transitions where *bad* is a BTOR2 operator that essentially specifies negated safety properties [36].

The selfie toolchain includes a RISC-U-to-BTOR2 translator called *BEATOR* that generates models in a subset of BTOR2 called BEATOR2 [28], as summarized in Table 2 including its usage and informal relation to RISC-U. Below, we nevertheless speak of BTOR2 rather than BEATOR2 despite the ambiguity. While BEATOR supports the *bad* operator, support of BTOR2 operators for specifying (global) fairness constraints and (negations of) liveness properties [36] is future work. BEATOR runs in time linear and generates models in space linear in the size of RISC-U code, and thus in the size of C* programs, such that:

BEATOR2 (\subset BTOR2)	Usage and Relation to RISC-U
sort bitvec size	value types (64-bit machine word and 1-bit Boolean)
sort array sort sort	memory type (64-bit elements, 64-bit address space)
Combinational Operators (related to SMT-LIB [4])	
constd sort integer	initial values, static addresses, immediate values
add sort $x y$	models add rd, x, y
sub sort $x y$	models sub rd, x, y
mul sort $x y$	models mul rd, x, y
udiv sort $x y$	models divu rd, x, y
urem sort $x y$	models remu rd, x, y
ult sort $x y$	models sltu rd, x, y
uext sort $x b$	unsigned extension of ult, input to 64-bit words
slice sort $x u l$	address down-scaling $u - l + 1$ bits from bit l to bit u
ite sort bool $x y$	ite cascades over pc flags for state updates
and sort bool bool	control flow of beq and jalr
not sort bool	jalr, false branch of beq
eq sort $x y$	jalr, true branch of beq
+ neq, ulte, ugt(e)	bound checks, kernel model
read sort mem idx	models ld rd, idx
write sort mem idx val	models sd val, idx
Sequential Operators (not in SMT-LIB [4])	
state sort name	variable of sort with name
init sort state val	initial value val of state
next sort state val	transition of state to val
input sort	symbolic input variable used in READ syscall model
bad bool	bool describes error state

Table 2. Table of all BEATOR2 declarations and combinational and sequential operators [28] from BTOR2 [36]

PROPOSITION 3.1. *Given a C^* program P , the RISC-U code R generated from P runs into an error state for an input I after executing n instructions if and only if a bad state in the BTOR2 model generated by BEATOR for R is reachable on I in $n + |I|$ state transitions (reading input in RISC-U only takes a single ecall instruction whereas in the BTOR2 model reading input takes multiple transitions bounded in $|I|$ modeling the ecall).*

An error state is a non-zero exit code, division by zero, and segmentation faults, that is, any, possibly input-dependent memory access outside of the data, heap, and stack segments. We added checking for segmentation faults to BEATOR to support QUBO modeling of memory access. Optionally, BEATOR can also generate additional checks such that memory accesses outside of memory blocks allocated by malloc are error states. However, those checks increase the size of the BTOR2 model by around 50%.

The key idea of BEATOR is to separate control and data flow in RISC-U code as follows. For data flow, BEATOR generates zeroed 64-bit bitvectors, one for each general-purpose register, and an array of zeroed 64-bit bitvectors, one for each 64-bit memory word, indexed by a 64-bit bitvector as memory address. The array models RISC-U main memory where the data and stack segments are initialized exactly as a RISC-U bootloader initializes them prior to code execution. This also includes the stack pointer which is the only register that must be initialized by the bootloader. We enhanced BEATOR with support of a down-scaled linear address space and a segmenting MMU and RAM model that

```

1 sort bitvec 1 ; Boolean
2 sort bitvec 64 ; 64-bit machine word
3 sort array 2 2 ; 64-bit physical memory
10 zero 1 ...
//... register states 200-231 ...
200 zero 2 zero // reg. $0 always 0 ...
203 state 2 gp ; register $3 ...
205 state 2 t0 ; register $5
206 state 2 t1 ; register $6
//... program counter states ...
16603600 state 1 // beq t0,zero,8[R0]
16603601 init 1 16603600 10
16604000 state 1 // A0:ld t0,-16(gp) ...
16606800 state 1 // R0:addi t0,zero,0
//... 64-bit memory (data,heap,stack):
20000000 state 3 physical-memory
    loading data,heap,stack into memory:
20000001 init 3 20000000 17380002
//... data flow ... A0:ld t0,-16(gp):
36604000 constd 2 -16
36604001 add 2 203 36604000
36604003 read 2 20000000 36604001
36604004 ite 2 16604000 36604003 36603202
//... A1:add t0,t0,t1:
36605600 add 2 205 206
36605601 ite 2 16605600 36605600 36604004
//... SEGFL:ld t0,0(t0):
36606002 ite 2 16606000 36606001 36605601
//... R0:addi t0,zero,0:
36606800 ite 2 16606800 200 36606002
//... updating registers ...
60000005 next 2 205 36606800 t0

```

Fig. 5. Data-flow fragment of the BTOR2 model for the running example

avoids arrays of bitvectors. QUBOT also models MMU and RAM which allows us to tradeoff translation complexity, as described in the next section and in Section 5.

For control flow, BEATOR generates zeroed 1-bit bitvectors, called pc flags, one for each instruction in the RISC-U code, for modeling the program counter. The pc flag for the instruction at the entry point of the code is the only pc flag initialized to 1 indicating that this instruction is the first to execute. From then on, control flows through the model by resetting the pc flag of the current instruction, after executing it, and then setting the pc flag of the next instruction to execute. Thus the invariant here is that at all times all pc flags are 0 except one. The alternative to pc flags is to represent the program counter explicitly by a 64-bit bitvector (32 bits are actually enough here but require scaling) and then control execution of instructions by comparing that bitvector with their constant addresses in memory. The advantage is that we only need one fixed-size bitvector instead of as many pc flags as there are instructions. However, model size still remains linear in code size and model checking performance may be negatively affected too. Exploring that alternative, also in QUBOT, remains future work.

```

11 one 1
//... data flow ...
36603600 eq 1 205 200 // $t0==$zero
36603601 not 1 36603600 // $t0!=$zero
//... control flow ...
//          beq t0,zero,8[R0]:
56603600 next 1 16603600 16603200
//          A0:ld t0,-16(gp):
56604000 and 1 16603600 36603601
56604001 next 1 16604000 56604000
// ...          sd t0,-8(s0):
56606400 next 1 16606400 16606000
// ...          R0:addi t0,zero,0:
56606800 and 1 16603600 36603600
56606801 ite 1 56606800 11 16606400
56606802 next 1 16606800 56606801

```

Fig. 6. Conditional control-flow fragment of the BTOR2 model for the running example

Consider Fig. 5 which shows a data-flow fragment of the BTOR2 model generated from the running example in Fig. 2. In BTOR2, comments are single-line comments that begin with a semicolon. Comments that begin with a double slash are not BTOR2 format and only inserted by us by hand for documentation. Each line begins with a node (line) identifier (nid) which must be larger than any previous nid. After the nid there is a keyword that identifies a BTOR2 operator followed by its arguments which may only be nids and integer literals. Forward references to larger nids than the current nid are not allowed.

The model begins with sort (type) declarations of pc flags and memory word bitvectors as well as the memory array in nids 1–3. Sorts are applied strictly by btormc which turns out to be helpful for debugging BEATOR. The 2 2 in line 3 sort array 2 2 refer to nid 2 as the index and element sorts of the array. Line 10 zero 1 declares the constant 0 of sort 1-bit bitvector. Lines 200–231 declare state variables for the 32 registers 0–31. Next are zeroed state declarations of the pc flags where each nid begins with digit 1, followed by the address of the instruction in decimal at runtime, followed by 00 and 01 for declaration and initialization, respectively. For example, the line at nid 16603600 declares the pc flag for beq t0,zero,8[R0] which is stored in memory at 0x101F4 or 66036 in decimal. Memory is declared in 20000000 state 3 physical-memory and initialized in 20000001 init 3 20000000 17380002 where nid 17380002 refers to the initial state of memory (not shown).

Then, there are ite (if-then-else) cascades that encode per-instruction data flow where each nid begins with digit 3, followed by an ite expression that either selects the data flow of the given instruction, if its pc flag is set, or else refers to the data flow of the closest previous instruction that updates the same state variable. For example, 36606800 ite 2 16606800 200 36606002 either selects the value of register zero (nid 200) for updating the value of register t0, if R0:addi t0,zero,0 is currently executing (nid 16606800), or else refers to the ite expression for SEGFL:ld t0,0(t0) at 36606002 which may also update t0, and so on. Finally, the next value of registers such as t0 at nid 205 is determined by lines whose nids begin with digit 6 such as 60000005 next 2 205 36606800 t0 which refers to the head of the ite cascade for t0 at 36606800. Actual computation can be seen in 36605600 add 2 205 206 which adds the values of registers t0 and t1 (nid 206) as instructed by A1:add t0,t0,t1. Line 36604003 read 2 20000000 36604001 models the memory read at address gp-16 as instructed by A0:ld t0,-16(gp).

```

20 zero 2 ...
22 constd 2 2 ...
//... 1-byte input
71 sort bitvec 8 ; 1 byte ...
81 input 71 ; 1 byte ...
91 uext 2 81 56 // extd. input to 64 bits
//... register states ...
202 state 2 sp ; register $2 ...
210 state 2 a0 ; register $10
211 state 2 a1 ; register $11
//... read system call ...
42000001 ite 2 42000000 211 36609200 ...
42000007 eq 1 42000006 22 // inc == 2
42000008 ite 2 42000007 92 91 ...
42000019 eq 1 42000006 28 // inc == 8
42000020 ite 2 42000019 98 42000018
42000021 add 2 211 210 ; $a1 + $a0
// memory[$a1 + $a0] = input:
42000022 write 3 20m 42000021 42000020
//... brk system call:
45000001 state 2 brk-bump-pointer
//... updating physical memory:
70000000 next 3 20000000 42000028
//... address >= current end of heap:
80000006 ugte 1 44000001 45000001
// address < current start of stack:
80000007 ult 1 44000001 202
80000008 and 1 80000006 80000007
// access between heap and stack:
80000009 bad 80000008 b2

```

Fig. 7. System call and bad state fragment of the BTOR2 model for the running example (20m stands for 20000000)

Fig. 6 shows a conditional control-flow fragment of the BTOR2 model generated from the running example in Fig. 2. For example, line 56606802 next 1 16606800 56606801 sets the pc flag of R0: addi t0, zero, 0 (nid 16606800) either if beq t0, zero, 8[R0] is currently executing (its pc flag at nid 16603600 is set) and the value of register t0 is equal to 0 (line at nid 36603600), or else if sd t0, -8(s0) is currently executing (pc flag at nid 16606400 and the line at nid 56606801). If beq t0, zero, 8[R0] is currently executing and the value of register t0 is not equal to 0 (line at nid 36603601) then the pc flag of A0: ld t0, -16(gp) is set (line at 56604001). Note that only the translation of beq as well as jal and jalr instructions results in BTOR2 code that *connects* control and data flow. While there are only finitely many jump targets with jal and jalr instructions (RISC-U binaries are static), beq instructions remain as the only source of path explosion with read system calls being the only source of data explosion, as shown next.

Lastly, Fig. 7 shows a system call and bad state fragment of the BTOR2 model generated for the running example. In particular, it shows how input flows into the model through a read system call, how a potential segmentation fault is detected as bad state, and how main memory is written to, in this case, through the read system call. One-byte input (nid 81) is unsigned-extended to a 64-bit memory word (nid 91) and then flows via an ite cascade (head at nid 42000020) to a write operator (nid 42000022). The address for the write operator is a1 + a0 (nid 42000021) where register a0 (nid 210) is a cursor over the write buffer that was originally passed to the read system call in register

a1 (nid 211). A potential segmentation fault, such as through `SEGFL:ld t0,0(t0)`, is detected in line 80000009 bad 80000008 b2 if there is any memory access at an address above the heap (bump pointer value of the `brk` system call at nid 45000001) and below the stack (pointer nid 202) where nid 44000001 is the head of an `ite` cascade over all addresses used in `read` and `write` operators. There are similar bad states for other unsafe parts of memory. All of main memory is updated by a single `next` (nid 70000000) that refers to the head of an `ite` cascade at 42000028 over all `write` operators in the model.

There is a fun fact that we like to mention: running BEATOR is fast and since it is written in C* it can actually model itself and the rest of the selfie toolchain written in C* as well. The BTOR2 model of the whole C* toolchain takes less than a second to build and is around 4MB.

3.4 BEATOR Loves QUBOT Loves BEATOR

Dead code elimination, constant propagation, and *bounded memory modeling* are all effective translation techniques in reducing the number of qubits in a QUBO model. Moreover, they can be done by BEATOR or by QUBOT. We have therefore enhanced BEATOR with support of all three. By bounded memory modeling we mean modeling a segmenting MMU and RAM in a bounded number of 64-bit bitvectors, one for each memory word in RAM, resulting in BTOR2 models that do not contain any arrays of bitvectors and thus any `read` and `write` operators anymore. The segmenting MMU bounds the size of the data, heap, and stack segments and then maps them, using the `slice` operator of BTOR2, from the 64-bit RISC-U virtual address space to a minimal physical address space. For the running example, a 4-bit physical address space is sufficient with only 12 memory words actually being accessed: 2 data words, 1 heap word, and 9 stack words while only the heap word (`*x`) and 1 stack word (`a`) are ever updated, see again Fig. 4 for the memory layout.

The RAM option takes the MMU option further by mapping each access to a memory word onto the 64-bit RAM bitvectors. RAM removes the need for arrays of bitvectors but increases BEATOR’s complexity to $O(m|P|)$ where m is memory size. However, with RAM modeling already done in BEATOR, QUBOT’s complexity effectively remains the same, maintaining the toolchain’s complexity. The MMU option can be used without the RAM option and only reduces memory size without changing BEATOR’s complexity. We have also implemented a third, combined MMURAM option in BEATOR that mimics QUBOT’s implementation which maps virtual addresses directly to the 64-bit RAM bitvectors.

Constant propagation in BEATOR runs in $O(n)$ time by executing the first n RISC-U instructions of a binary until reaching the first `read` call. Then, BEATOR eliminates dead code and snapshots the machine state including the heap as initial state in the BTOR2 model. QUBOT takes advantage of the additional $O(n)$ time, maintaining the toolchain’s complexity, and propagates constants beyond the first `read` call. However, propagating constants until the first `read` call is faster in BEATOR. Quantitative details are in Section 5.

4 QUANTUM MODELING WITH QUBOT

We introduce, by continuing to use the running example, the BTOR2-to-QUBO translator called *QUBOT* which is our main technical contribution, besides the enhancements to BEATOR. A QUBO model is a binary quadratic (BQ) function, which QUBOT generates from a BTOR2 model. A BQ function is a quadratic function from binary variables to positive real values and 0 (ground energy on a quantum annealer). Constant factors are signed real values that are eventually normalized before solving the function. For example, the BQ function that encodes the logic gate for $NOT(x) = y$ is:

$$NOT_{BQ}(x, y) = 2 - 2x - 2y + 4xy$$

BEATOR2 (\subset BTOR2)	#Binary Variables (Qubits)
sort bitvec, array	0
Combinational Operators (related to SMT-LIB [4])	
constd	only constants
add, sub	$O(w)$ circuit
mul	$O(w^2)$ circuit
udiv, urem	$O(w^2)$ constrained circuit
uext	only constants
slice	0
ite, and, not, eq	$O(w)$ circuit
neq, ult(e), ugt(e)	$O(w)$ circuit
read, write	$O(wm)$ circuit
Sequential Operators (not in SMT-LIB [4])	
state, input	$O(w)$ variables
init	only constants
next	0 in circuit
bad	1 in constrained circuit

Table 3. QUBO model size with respect to BEATOR2 declarations and operators [28] where w is machine word size (here 64) and m is memory size

Try evaluating the function to see when it reaches ground energy! Instead of generating a file, QUBOT represents a QUBO model as upper-diagonal matrix of constant factors in memory using a Python library by D-Wave Systems². The diagonal of the matrix represents linear factors such as $-2x$ and the upper part represents bi-linear factors such as $4xy$. Quadratic factors of binary variables such as $-2x^2$ are actually linear factors⁴ because $-2x^2 = -2x$. The model may be output in various formats including visualizations, see Fig. 8. QUBOT runs in $O(n^2)$ time and space such that:

PROPOSITION 4.1. *Given a C^* program P and a bound n , there is input I on which a bad state is reachable in no more than n state transitions in the BTOR2 model B generated by the C^* compiler and BEATOR for P if and only if the QUBO model generated by QUBOT for B and n evaluates to 0 on I .*

Thus, with more qubits q on the machine than variables in the QUBO model, quantum annealing the model reaches 0 (ground) energy in constant time with high probability on some input I that is part of the ground state if and only if a bad state is reachable in B on I in no more than n state transitions. Otherwise, if q is insufficient, annealing may still work in $O(n^2/q)$ time using a hybrid solver [30]. The size of the model comes down to $O(n \cdot |P|)$ if memory consumption of P is bounded by a constant.

The key challenge in the translation is to encode reachability in a state machine (BTOR2 model) in a stateless BQ function (QUBO model). Before learning how QUBOT translates our running example, let us focus on the fact that any combinational circuit can be represented by a BQ function:

PROPOSITION 4.2. *Let x , y , and z be binary variables and let f be a function (logic gate) that maps x and y to z . There exists at least one BQ function g over x , y , and z such that $g(x, y, z) = 0$ if and only if $f(x, y) = z$ for all x , y , and z in $\{0, 1\}$.*

For example, for all x , y , and z in $\{0, 1\}$, $AND(x, y) = z$ if and only if $6z + 2xy - 4xz - 4yz = 0$. Even though AND and NOT are universal, we also use dedicated BQ functions for $NAND$, OR , and $AND(NOT(x), y)$ (inhibition) for

⁴thus BQ functions are actually binary bi-linear functions

encoding the combinational operators in BTOR2. Similar to SMT solvers such as Z3 [17] and boolector [35], QUBOT uses (polynomial) bit blasting except for `udiv` and `urem` which are reduced to constraints over multiplication. However, since solving those constraints is expensive, QUBOT cannot efficiently validate QUBO models generated from `udiv` and `urem`. Bit blasting both operators is future work. Memory access through `read` and `write` is bit-blasted, see below for more details. Note that composing a function from multiple BQ functions that generally share variables is straightforward using addition since the composed function is again a BQ function from binary variables to positive values and 0. Table 3 provides a summary of the size of the BQ functions for all BTOR2 operators in terms of the size w of a machine word (here 64) and the size m of memory.

The key idea of QUBOT is to model, given a bound n , the input I and state variables S in a BTOR2 model in $\mathcal{O}(n)$ qubits (binary variables) that are biased and entangled with another set of $\mathcal{O}(n)$ qubits that represent the output of the combinational circuits for control and data flow on I and S . At least logically that model is then duplicated n times where, for all $0 \leq i < n$, duplicate D_i is entangled with duplicate D_{i+1} such that each qubit o in D_i that represents an output of a combinational circuit in the BTOR2 model is used in D_{i+1} as qubit that represents the part of the state variable in the BTOR2 model which o updates [37]. Input variables are introduced in each duplicate as uninitialized state variables. After that, constants and initial values of initialized state variables are propagated at bit level (not word level) through the model.

This is the logic. In reality, QUBOT builds the model incrementally propagating constants as soon as possible to keep the model from growing unnecessarily. Instead of duplicating D_i , the model for D_{i+1} is built from scratch, one combinational circuit per next operator at a time, immediately followed by propagating constants through that circuit. However, there is an issue: a qubit o that represents an output of a circuit must not be replaced by a constant before all its future entanglements (uses) are known and have been modeled, which in the worst case may happen at $i = n - 1$. The reason is that o might represent part of a state variable not just in D_{i+2} but also later until that part of the state variable is updated again by a qubit other than o . In short, state is memory (registers), and memory that is not updated keeps its value. Thus QUBOT remembers each such qubit o and its possibly known constant value until it can be applied safely.

Incremental constant propagation in QUBOT is highly effective—all state variables including all pc flags are initialized—but it is certainly not exhaustive. Static analysis techniques other than constant propagation for further reducing the number of qubits may apply as well but remain future work. One such opportunity in the running example is the subtraction in `a = a - 1` in the body of the while loop. If the loop condition `a > '0'` was known at the time of subtraction, the bit resolution of the data flow through variable `a` could remain at 8 bits rather than 64 bits because `a - 1` never overflows into the 56 more significant bits. However, through mere constant propagation QUBOT is currently unable to perform that reasoning. Nevertheless, note that constant propagation enables QUBOT to validate models on known inputs efficiently, see Section 5.

Let us now go through the running example from QUBOT's perspective. Given a BTOR2 model such as the model for our running example, QUBOT only looks for `next` and `bad` operators. For each line with a `next` operator, such as `60000005 next 2 205 36606800 t0` for data flow into registers in Fig. 5 and `70000000 next 3 20000000 42000028` for data flow into memory in Fig. 7, and `56606802 next 1 16606800 56606801` for control flow in Fig. 6, QUBOT builds the BQ functions for the referenced (here, 64-bit and 1-bit bitvector) combinational circuits recursively, here `nids 36606800`, `42000028`, and `56606801`, respectively. Lines with state, input, and `constd` operators terminate the recursion. When building D_0 , QUBOT also looks for lines with `init` operators that initialize the encountered state variables and then, together with the encountered `constd` constants, performs constant propagation as described above. For each line with a `bad` operator, such as `80000009 bad 80000008 b2` for detecting potential segmentation faults in

Fig. 7, QUBOT again builds the BQ function for the referenced (1-bitvector) combinational circuit recursively, here nid 80000008, and then constrains the BQ function in an *OR* circuit over all BQ functions generated for lines with bad operators to 1 (true).

Updating memory through the line 70000000 next 3 20000000 42000028 in Fig. 7 works just like any other line with a next operator, except that the referenced (array) combinational circuit involves read and write operators. The issue with these operators is that QUBOT generates a BQ function that compares the referenced (64-bit bitvector) address, such as nid 42000021 in the line 42000022 write 3 20000000 42000021 42000020, with all addresses of the entire memory to identify the correct memory word, which is then read or written, here with the output of the referenced (64-bit bitvector) combinational circuit (nid 42000020).

In order to address scalability, QUBOT maps virtual addresses to a minimal physical address space at translation time, similar to the combined MMURAM option in BEATOR. Here, BEATOR generating bad states for detecting segmentation faults in the BTOR2 model frees QUBOT from checking again. For the running example, a 4-bit physical address space for 12 memory words is sufficient, see again Fig. 4 for the memory layout. Most importantly, constant propagation in QUBOT reduces BQ functions modeling memory access via constant addresses to BQ functions modeling register access, effectively making their size independent of memory size. While we discussed QUBOT’s perspective on a BTOR2 model generated by the selfie toolchain, we should mention that QUBOT is able to handle any model within the BEATOR2 subset of BTOR2 and thus enables bounded model checking in general within the theory of bitvectors and arrays of bitvectors on a quantum annealer.

In sum, given a C* program P and a bound n , the full selfie toolchain takes $O(n^2)$ time to generate a QUBO model for P where generating each D_i for $0 \leq i < n$ takes $O(n)$ time. That time reduces to $O(|P|)$ if memory consumption of P is bounded by a constant, establishing the main principled contribution of this paper:

PROPOSITION 4.3. *Algorithmic time (space) of an algorithm in classical computing is a linear (quadratic) upper bound on quantum space in number of qubits for running the algorithm on a quantum annealer.*

An immediate consequence of that result is that any (evidential) program P that checks in polynomial time (executing n instructions) whether some input I is a solution to a problem in NP can be translated in $O(n^2)$ time to an $O(n^2)$ QUBO model that evaluates to 0 on I in constant time on a quantum annealer with sufficiently many qubits, providing a non-relativizing proof of:

COROLLARY 4.4. $NP \subseteq BQP$

This result does not contradict the optimality of Grover’s algorithm [23] which can here be seen as treating the $O(n^2)$ QUBO model as black box computing I in $O(\sqrt{n^2})$, that is, $O(n)$ steps with high probability through the control-flow graph in the model asking an oracle for directions, just like our toolchain and a quantum annealer.

4.1 Quantum Advantage

In the following, we define a quantitative notion of quantum advantage for quantum annealing machines and argue how that can potentially be leveraged in a hybrid solver based on QUBOT. Recall that we use the terms qubit and binary variable as synonyms. We first define the *status* of a qubit in a QUBO model Q_n created by our toolchain for a C* program P and a bound n . The status can be determined by a (classical) SMT solver that has access to the BTOR2 model from which Q_n has been generated:

Definition 4.5. Given a C^* program P , a bound n , and a classical time budget $T \geq 0$, we say that a qubit b in Q_n is *T-determined* (or *T-approximated*) if the value of b can be determined within T classical time to be either 0 or 1 for all (or some) inputs of Q_n . We say that b is in *T-superposition* if the value of b can be T -approximated to be 0 for some input of Q_n and 1 for some other input of Q_n . We say b is *T-undetermined* if b is neither T -determined nor in T -superposition.

Note that qubits that represent inputs of a QUBO model are in T -superposition for any time budget. Next, we assume that in all QUBO models the status of qubits has been determined and all qubits that are T -determined to a value have been replaced by that value. In other words, in all QUBO models all qubits are either in T -superposition or T -undetermined. By $|Q_n|$ and $|Q_n|_T$ we denote the total (excluding T -determined qubits) and T -undetermined number of qubits, respectively.

Definition 4.6. Given a C^* program P , a classical time budget $T \geq 0$, and a qubit capacity $C \geq |Q_0|$, the *quantum advantage* of P is n state transitions (classical time) and q qubits (quantum space) where $q = C - |Q_i|$ for some $i \geq 0$ such that $|Q_i|_T = 0$, $|Q_{i+1}|_T > 0$, $|Q_{i+n}| \leq C$, and $|Q_{i+n+1}| > C$.

Intuitively, the quantum advantage of a program is the number of state transitions and qubits that are T -undetermined or in T -superposition before running out of qubits on a quantum annealer and after exhausting our classical time budget in determining qubit status. In turn, this means that the faster our classical SMT solver determines at least qubit status the harder it is to gain quantum advantage. Worse, quantum advantage can even be negative ($n, q < 0$) indicating that we ran out of qubit capacity even before introducing any T -undetermined qubits. In that case, classical symbolic execution and bounded model checking is our only option.

However, we can gain further *incomplete (but sound) quantum advantage* by replacing T -undetermined qubits by values to which they can at least be T -approximated. This may even be done in a feedback loop with a quantum annealer that provides T -approximations instead of an SMT solver. The result is a hybrid QUBOT solver that can then reuse T -approximated qubits, resembling failed literal detection [9, 19], possibly preventing n and q to ever become negative. In that setting, restoring completeness efficiently may nevertheless be hard because there can be exponentially many T -approximations (variable assignments).

4.2 Quantum Advantage Processing Unit (QAPU)

Given a C^* program P , imagine a *quantum advantage processing unit* (QAPU) made up of a quantum annealer (combinational part) and quantum memory (sequential part) where the quantum annealer is configured to anneal the uninitialized (!) QUBO model duplicate D_1 generated by QUBOT for P and 1, and the quantum memory is initialized to the initial QUBO model D_0 for P and 0. We then say that D_0 and D_1 are the QAPU program for P , and its execution on a QAPU in n quantum annealing steps is the full QUBO model generated by QUBOT for P and n :

PROPOSITION 4.7. *Given a C^* program P , there is input I on which a bad state is reachable in n state transitions in the BTOR2 model generated by BEATOR for P if and only if the execution of the QAPU program for P on a QAPU evaluates to 0 on I in n quantum annealing steps.*

The selfie toolchain takes $O(n)$ time to generate the QAPU program for P where n is a bound on the number of executed instructions and thus memory consumption by P . Translation time and QAPU program size reduce to $O(|P|)$ if memory consumption of P is bounded by a constant, establishing our final result:

PROPOSITION 4.8. *Algorithmic space of an algorithm in classical computing is a linear upper bound on quantum space in number of qubits for running the algorithm on a quantum advantage processing unit.*

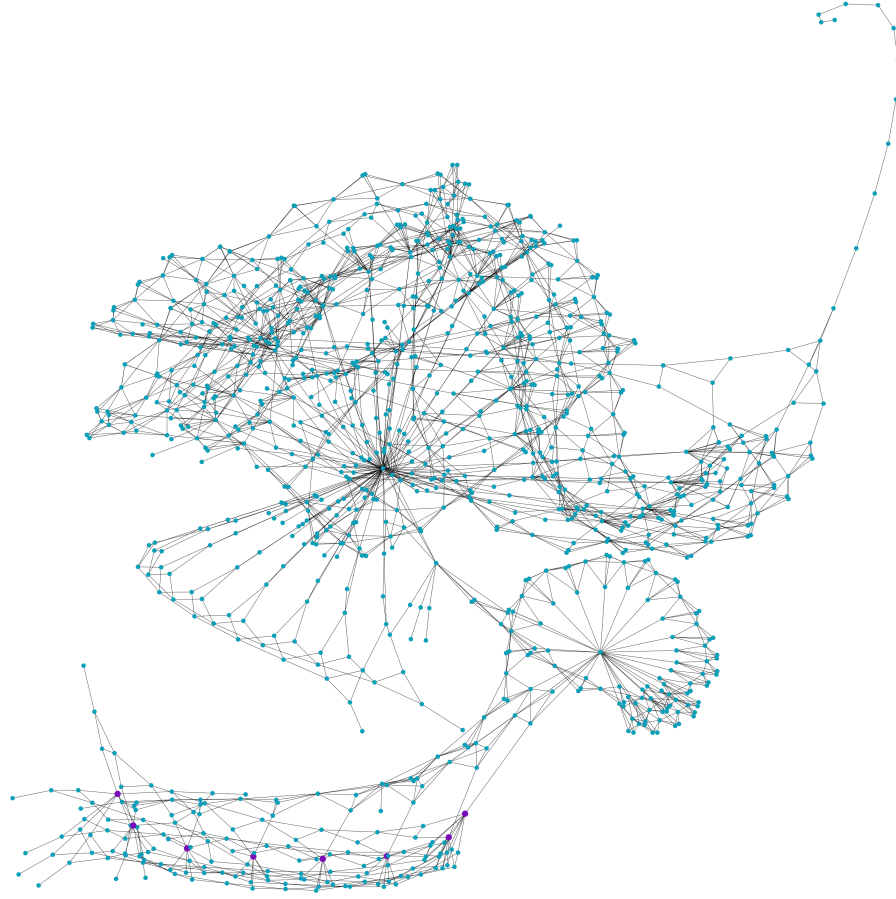


Fig. 8. QUBO model of the running example with 15 state transitions (input qubits are purple in lower left corner, bad states—segfault!—are the tail in upper right corner)

In sum, a quantum computer with a QAPU is universal and may execute any C* program P that uses fewer classical bits in CPU registers and memory than there are qubits in QAPU annealer and memory. Also, a QAPU may only run P at the exact same algorithmic complexity of P when running on a CPU. So, where is the quantum advantage then? Well, a QAPU executes P for *all* inputs whereas a CPU only executes P for *one* input. As mentioned in the introduction, we may eventually leverage that through evidential programming where P merely checks, say, in linear time, if an input is a solution to a problem rather than computes a solution. Now it appears that, other than saving qubits in QUBO models, the "only" thing left to do is to build a QAPU with as many qubits as possible providing quantum advantage for all!

5 EXPERIMENTS

First of all, we managed to run real 64-bit C code on D-Wave's 4.1 5k-qubit quantum annealer! While we had to replace the code below the assignment $a = *x$; in the running example with just one assignment $a = *(x + a)$; , which may trigger a segmentation fault for all inputs other than 0, we still feel that this is another breakthrough and, to the best of our knowledge, the first time C code, using dynamic memory allocation (as simple as it might be) and not targeting

BEATOR Config.	KB	Time (s)	#Qubits (k)
DEFAULT	51[50]	21+8[11+4]	217[109]
LINEAR	53[52]	21+8[11+4]	197[108]
MMU	78[77]	23+9[12+4]	245[126]
RAM	136[135]	174+52[97+29]	1190[618]
MMURAM	100[99]	25+9[12+5]	234[118]
CONST-PROP	33[32]	6+3[3+1]	143[72]
CONST-LIN	34[33]	6+2[3+1]	130[72]
CONST-MMU	47[46]	8+3[4+2]	194[101]
CONST-RAM	69[68]	27+12[15+6]	685[346]
CONST-MR	52[51]	9+4[4+2]	180[92]
12BAD	50[49]	18+7[10+4]	215[108]
12BAD-LIN	51[50]	18+7[9+3]	196[107]
12BAD-MMU	77[75]	19+7[10+4]	243[125]
12BAD-RAM	135[133]	173+51[97+28]	1188[618]
12BAD-MR	99[98]	22+8[11+4]	233[117]
12BAD-CONST	31[30]	5+2[3+1]	142[72]
12BAD-C-LIN	32[31]	5+2[3+1]	128[71]
12BAD-C-MMU	46[45]	7+3[4+2]	193[100]
12BAD-C-RAM	68[67]	26+11[15+6]	684[345]
12BAD-C-MR	51[49]	8+3[4+2]	178[91]

Table 4. BEATOR2 model size in kilobyte (KB), QUBOT translation time in seconds (modeling time + constant-propagation time), number of generated qubits in thousands, 32-bit results in brackets (obtained with running example)

quantum annealers [24], ran on a quantum computer through a fully automated toolchain. Fig. 8 visualizes a QUBO model of the unmodified running example for 15 state transitions.

The goal of our experiments is to establish confidence in correctness through validation of QUBO models and to understand performance tradeoffs between BEATOR and QUBOT. Table 4 shows, for the running example, BEATOR2 model size in kilobyte (KB), QUBOT translation time in seconds (model build time + constant propagation time), number of generated qubits in thousands, and 32-bit results in brackets. We interpret the data as follows: (1) the lowest QUBOT translation time and qubit count is reached if BEATOR, in decreasing order of efficacy, propagates constants until the first input is read (CONST-PROP), down-scales 64-bit virtual addresses to 29-bit [30-bit] linear addresses (LINEAR,LIN), and only generates bad states for segmentation faults (12BAD), (2) modeling MMU and RAM is more effective if done by QUBOT (on bit level versus on word level in BEATOR (MMU,RAM,MMURAM)), and (3) 32-bit models have, as expected, roughly half the qubit count of 64-bit models. We have run our toolchain on other examples and validated all QUBO models with similar results.

Constant propagation until first input is read is more effective in BEATOR than in QUBOT because the resulting program state is generally smaller. However, after that, constant propagation in QUBOT is highly effective, for example: 12BAD-C-LIN for 32-bit code results in around 3 million qubits without constant propagation in QUBOT. Downscaling to smaller linear address spaces is only slightly more effective in BEATOR than constant-propagating unused addressing bits in QUBOT while reducing the number of bad states in BEATOR has almost no effect. MMU and RAM modeling with constant propagation on bit level is generally more effective in QUBOT while support of 32-bit models can only be done in the toolchain before QUBOT.

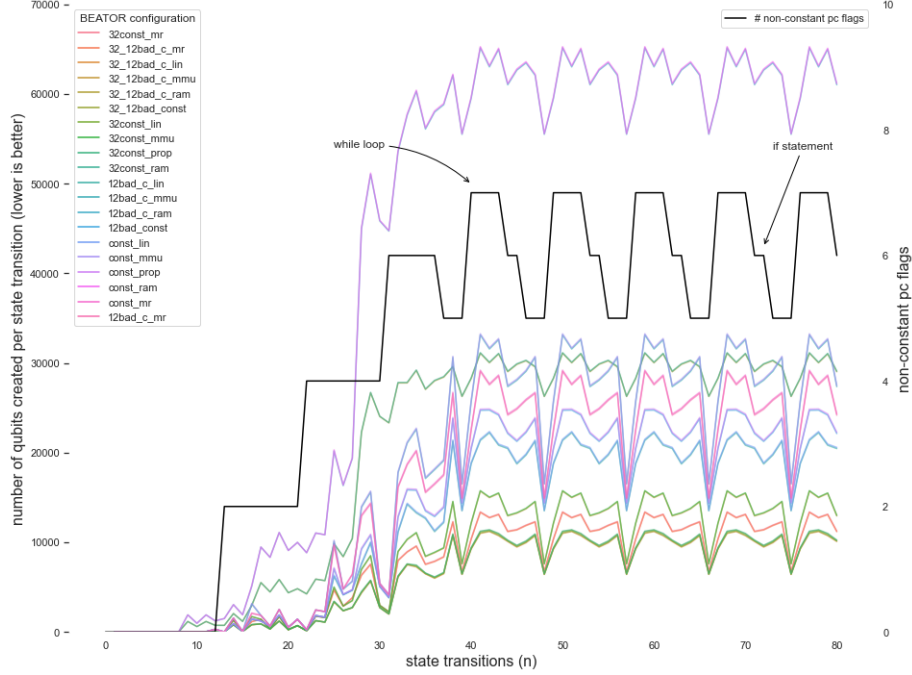


Fig. 9. Left y-axis: number of qubits per state transition (x-axis) for the running example (no growth is linear growth in total qubit count, data on 32-bit models is prefixed 32, the outliers at the top are BEATOR’s RAM configurations); right y-axis: number of non-constant pc flags (number of RISC-U instructions executed simultaneously, showing (linear) impact of the while loop and if statement on qubit count)

Fig. 9 shows the number of qubits created by QUBOT per state transition for the running example. Generally, the more effective BEATOR configurations result in slower qubit growth in QUBOT. Gaining quantum advantage essentially requires improving that data. The number of RISC-U instructions executed simultaneously (non-constant pc flags) beautifully shows the (linear) impact of control flow on qubit count, with the while loop and if statement showing up. For minor embeddings and QUBO model representation we have used D-Wave’s implementation. However, both aim at classical optimization problems and show performance issues with QUBOT that we plan to address with our own QUBOT-tailored design in future work.

6 CONCLUSIONS AND FUTURE WORK

Inspired by translation of classical code to quantum annealers [37] as well as symbolic execution through bounded model checking, we have shown how to translate RISC-V machine code compiled from C code to quadratic unconstrained binary optimization (QUBO) models that can be solved by a quantum annealer, establishing our main technical contribution: quantum annealing a QUBO model of a program P reaches 0 (ground) energy in constant time with high probability on some input I if and only if P runs on I into an error state such as division by zero executing no more than n instructions. Translation takes $O(n^2)$ time effectively turning a quantum annealer into a polynomial-time symbolic execution engine and bounded model checker. Translation time comes down to $O(n \cdot |P|)$ if memory consumption of P is bounded by a constant, establishing our main principled contribution: a linear (quadratic) upper bound on quantum space, in number of qubits on a quantum annealer, in terms of algorithmic time (space) in classical computing.

There are numerous directions for principled future work where outperforming, that is, gaining quantum advantage over classical symbolic execution and bounded model checking is at the top of the challenges. So far, we have dealt with the fundamental tradeoff between translation and annealing complexity by putting most hard, that is, exponential work into annealing. Any static analysis technique applied at translation time that scales to the linear (quadratic) upper bound is likely to produce significant progress in reducing the amount of qubits required to solve problems in practice. QUBO models play a key role in programming quantum annealers but may require more attention to be established as key abstraction from quantum physics, similar to the role of Boolean algebra in classical computing.

There are also numerous technical challenges of which we list just a few. Besides the obvious such as full C, RISC-V, and BTOR2 support, there is also need for support of floating-point arithmetic, more efficient handling of symbolic memory addresses, detection of properties other than safety, and more advanced system call handling that covers incorrect use of system calls. BEATOR could be bypassed entirely by translating RISC-V code directly to QUBO models while QUBOT could be generalized to a hybrid solver.

ACKNOWLEDGMENTS

We thank Armin Biere for inspiring us to build BEATOR! This work has been supported by the Czech Ministry of Education, Youth and Sports from the Czech Operational Programme Research, Development, and Education, under grant agreement No. CZ.02.1.01/0.0/0.0/15_003/0000421, and the European Research Council (ERC) under the European Union’s Horizon 2020 research and innovation programme, under grant agreement No. 695412.

REFERENCES

- [1] A.S. Abyaneh, S. Bauer, C.M. Kirsch, P. Mayer, C. Mösl, C. Poncelet, S. Seidl, A. Sokolova, and M. Widmoser. 2018. Selfie: Towards Minimal Symbolic Execution. In *Online Proc. Workshop on Modern Language Runtimes, Ecosystems, and VMs (MoreVMs)*.
- [2] A.S. Abyaneh and C.M. Kirsch. 2021. ASE: A Value Set Decision Procedure for Symbolic Execution. In *Proc. IEEE/ACM International Conference on Automated Software Engineering (ASE)*. IEEE/ACM.
- [3] Steven H. Adachi and Maxwell P. Henderson. 2015. Application of Quantum Annealing to Training of Deep Neural Networks. arXiv:1510.06356 [quant-ph]
- [4] C. Barrett, A. Stump, and C. Tinelli. 2010. The SMT-LIB Standard: Version 2.0. In *Proc. International Workshop on Satisfiability Modulo Theories*, A. Gupta and D. Kroening (Eds.).
- [5] G. Bass, M. Henderson, J. Heath, and J. Dulny. 2021. Optimizing the Optimizer: Decomposition Techniques for Quantum Annealing. *Quantum Mach. Intell.* (2021). <https://doi.org/10.1007/s42484-021-00039-9>
- [6] R. Battiti and M. Protasi. 1997. Reactive Search, a History-Sensitive Heuristic for MAX-SAT. *ACM J. Exp. Algorithmics* 2 (1 1997), 2–es. <https://doi.org/10.1145/264216.264220>
- [7] Z. Bian, F. Chudak, W. Macready, A. Roy, R. Sebastiani, and S. Varotti. 2017. Solving SAT and MaxSAT with a Quantum Annealer: Foundations and a Preliminary Report. In *Frontiers of Combining Systems*, C. Dixon and M. Finger (Eds.). Springer, Cham, 153–171.
- [8] A. Biere, A. Cimatti, E.M. Clarke, and Y. Zhu. 1999. Symbolic Model Checking without BDDs. In *TACAS (LNCS, Vol. 1579)*. Springer, 193–207.
- [9] A. Biere, M. Järvisalo, and B. Kiesl. 2021. Preprocessing SAT Solving. In *Handbook of Satisfiability* (second ed.), A. Biere, M. Heule, H. van Maaren, and T. Walsh (Eds.). Frontiers in Artificial Intelligence and Applications, Vol. 336. IOS Press, 391–435. <https://doi.org/10.3233/FAIA200992>
- [10] M.L. Bonet, J. Levy, and F. Manyà. 2007. Resolution for Max-SAT. *Artificial Intelligence* 171, 8 (2007), 606–618. <https://doi.org/10.1016/j.artint.2007.03.001>
- [11] K. Boothby, A. D. King, and A. Roy. 2020. Fast clique minor generation in Chimera qubit connectivity graphs. arXiv:1507.04774 [cs.DM]
- [12] C. Cadar, D. Dunbar, and D. Engler. 2008. KLEE: Unassisted and Automatic Generation of High-Coverage Tests for Complex Systems Programs. In *Proc. USENIX Conference on Operating Systems Design and Implementation (OSDI)*. USENIX Association, 209–224.
- [13] V. Chipounov, V. Kuznetsov, and G. Candea. 2011. S2E: A Platform for in-Vivo Multi-Path Analysis of Software Systems. In *Proc. International Conference on Architectural Support for Programming Languages and Operating Systems (ASPLOS)*. ACM, 265–278.
- [14] E. Crosson and A. W. Harrow. 2016. Simulated Quantum Annealing Can Be Exponentially Faster Than Classical Simulated Annealing. In *Proc. Annual Symposium on Foundations of Computer Science (FOCS)*. IEEE, 714–723. <https://doi.org/10.1109/FOCS.2016.81>
- [15] E. J. Crosson and D. A. Lidar. 2021. Prospects for Quantum Enhancement with Diabatic Quantum Annealing. *Nature Reviews Physics* 3, 7 (5 2021), 466–489. <https://doi.org/10.1038/s42254-021-00313-6>

- [16] P. Date, R. Patton, C. Schuman, and T. Potok. 2019. Efficiently Embedding QUBO Problems on Adiabatic Quantum Computers. *Quantum Information Processing* 18 (03 2019). <https://doi.org/10.1007/s11128-019-2236-3>
- [17] L. de Moura and N. Björner. 2008. Z3: An Efficient SMT Solver. In *Tools and Algorithms for the Construction and Analysis of Systems*, C. R. Ramakrishnan and Jakob Rehof (Eds.). Springer, 337–340.
- [18] A. Douglass, A. D. King., and J. Raymond. 2015. Constructing SAT Filters with a Quantum Annealer. In *Theory and Applications of Satisfiability Testing – SAT 2015*, M. Heule and S. Weaver (Eds.). Springer, Cham, 104–120.
- [19] J.W. Freeman. 1995. *Improvements to Propositional Satisfiability Search Algorithms*. Ph.D. Dissertation. University of Pennsylvania, PA, USA.
- [20] M. Gendreau and J. Potvin. 2005. *Tabu Search*. Springer, Boston, MA, 165–186. https://doi.org/10.1007/0-387-28356-0_6
- [21] F. Glover, G. Kochenberger, and B. Alidaee. 1998. Adaptive Memory Tabu Search for Binary Quadratic Programs. *Management Science* 44 (03 1998), 336–345. <https://doi.org/10.1287/mnsc.44.3.336>
- [22] E. Grant, T. S. Humble, and B. Stump. 2021. Benchmarking Quantum Annealing Controls with Portfolio Optimization. *Physical Review Applied* 15, 1 (1 2021). <https://doi.org/10.1103/physrevapplied.15.014012>
- [23] L.K. Grover. 1996. A Fast Quantum Mechanical Algorithm for Database Search. In *Proc. Symposium on Theory of Computing (STOC)* (Philadelphia, Pennsylvania, USA). ACM, New York, NY, USA, 212–219. <https://doi.org/10.1145/237814.237866>
- [24] M.W. Hassan, S. Pakin, and W. Feng. 2019. C to D-Wave: A High-level C Compilation Framework for Quantum Annealers. In *High Performance Extreme Computing Conference (HPEC)*. IEEE.
- [25] A. D. King and C. C. McGeoch. 2014. Algorithm engineering for a quantum annealing platform. arXiv:1410.2628 [cs.DS]
- [26] J.C. King. 1976. Symbolic Execution and Program Testing. *Commun. ACM* 19, 7 (1976), 385–394. <https://doi.org/10.1145/360248.360252>
- [27] C.M. Kirsch. 2017. Selfie and the Basics. In *Proc. ACM SIGPLAN International Symposium on New Ideas, New Paradigms, and Reflections on Programming and Software (Onward!)*. ACM.
- [28] C.M. Kirsch and M. Starzinger. 2022. Symbolic Execution versus Bounded Model Checking. In *Invited paper to appear in Festschrift 2022*. Springer.
- [29] G. Kochenberger, J. Hao, F. Glover, M. Lewis, Z. Lü, H. Wang, and Y. Wang. 2014. The Unconstrained Binary Quadratic Programming Problem: A Survey. *Journal of Combinatorial Optimization* 28 (07 2014). <https://doi.org/10.1007/s10878-014-9734-0>
- [30] K. Kurowski, J. Weglarz, M. Subocz, R. Rózycki, and G. Waligóra. 2020. Hybrid Quantum Annealing Heuristic Method for Solving Job Shop Scheduling Problem. In *Computational Science – ICCS 2020*, V. V. Krzhizhanovskaya, G. Závodszky, M. H. Lees, J. J. Dongarra, P. Sloot, S. Brissos, and J. Teixeira (Eds.). Springer, Cham, 502–515.
- [31] M. Lewis and F. Glover. 2017. Quadratic Unconstrained Binary Optimization Problem Preprocessing: Theory and Empirical Analysis. arXiv:1705.09844 [cs.AI]
- [32] A. Lucas. 2014. Ising formulations of many NP problems. *Frontiers in Physics* 2 (2014). <https://doi.org/10.3389/fphy.2014.00005>
- [33] J. C. Meza. 2010. Steepest Descent. *WIREs Computational Statistics* 2, 6 (2010), 719–722. <https://doi.org/10.1002/wics.117>
- [34] A. Misevicius. 2005. A Tabu Search Algorithm for the Quadratic Assignment Problem. *Computational Optimization and Applications* 30 (01 2005), 95–111. <https://doi.org/10.1007/s10589-005-4562-x>
- [35] A. Niemetz, M. Preiner, and A. Biere. 2015. Boolector 2.0 System Description. *Journal on Satisfiability, Boolean Modeling and Computation* 9 (2015), 53–58.
- [36] A. Niemetz, M. Preiner, C. Wolf, and A. Biere. 2018. Btor2, BtorMC and Boolector 3.0. In *Computer Aided Verification*, H. Chockler and G. Weissenbacher (Eds.). Springer, 587–595.
- [37] S. Pakin. 2019. Targeting Classical Code to a Quantum Annealer. In *Proc. International Conference on Architectural Support for Programming Languages and Operating Systems (ASPLOS)*. ACM. <https://doi.org/10.1145/3297858.3304071>
- [38] G. Paul. 2011. An Efficient Implementation of the Robust Tabu Search Heuristic for Sparse Quadratic Assignment Problems. *European Journal of Operational Research* 209 (03 2011), 215–218. <https://doi.org/10.1016/j.ejor.2010.09.009>
- [39] E. Pelofske, J. Golden, A. Bärtschi, D. O’Malley, and S. Eidenbenz. 2021. Sampling on NISQ Devices: “Who’s the Fairest One of All?”. arXiv:2107.06468 [quant-ph]
- [40] O. Shylo, D. Korenkevych, and P. Pardalos. 2012. Global Equilibrium Search Algorithms for Combinatorial Optimization Problems. 277–286. https://doi.org/10.1007/978-3-642-32964-7_28
- [41] V. P. Shylo and O. V. Shylo. 2010. Solving the Maxcut Problem by the Global Equilibrium Search. *Cybernetics and Systems Analysis* 46, 5 (01 9 2010), 744–754. <https://doi.org/10.1007/s10559-010-9256-4>
- [42] J. Su, T. Tu, and L. He. 2016. A Quantum Annealing Approach for Boolean Satisfiability Problem. In *Proc. ACM/EDAC/IEEE Design Automation Conference (DAC)*. 1–6. <https://doi.org/10.1145/2897937.2897973>
- [43] Z. Tabi, K. H. El-Safty, Z. Kallus, P. Haga, T. Kozsik, A. Glos, and Z. Zimboras. 2020. Quantum Optimization for the Graph Coloring Problem with Space-Efficient Embedding. *Proc. International Conference on Quantum Computing and Engineering (QCE)* (10 2020). <https://doi.org/10.1109/qce49297.2020.00018>
- [44] R. Tanburn, E. Okada, and N. Dattani. 2015. Reducing multi-qubit interactions in adiabatic quantum computation without adding auxiliary qubits. Part 1: The “deduc-reduc” method and its application to quantum factorization of numbers. arXiv:1508.04816 [quant-ph]
- [45] H. Ushijima-Mwesigwa, C. F. A. Negre, and S. M. Mniszewski. 2017. Graph Partitioning using Quantum Annealing on the D-Wave System. arXiv:1705.03082 [quant-ph]

- [46] H. M. Waidyasooriya and M. Hariyama. 2020. A GPU-Based Quantum Annealing Simulator for Fully-Connected Ising Models Utilizing Spatial and Temporal Parallelism. *IEEE Access* 8 (2020), 67929–67939. <https://doi.org/10.1109/ACCESS.2020.2985699>
- [47] B. Wang, F. Hu, H. Yao, and C. Wang. 2020. Prime Factorization Algorithm Based on Parameter Optimization of Ising Model. *Scientific Reports* 10 (04 2020). <https://doi.org/10.1038/s41598-020-62802-5>
- [48] A. Waterman, Y. Lee, D.A. Patterson, and K. Asanović. 2016. *The RISC-V Instruction Set Manual, Volume I: User-Level ISA, Version 2.1*. Technical Report UCB/EECS-2016-118. EECS Department, University of California, Berkeley. <http://www2.eecs.berkeley.edu/Pubs/TechRpts/2016/EECS-2016-118.html>
- [49] S. Weaver, K. Ray, V. Marek, A. Mayer, and A. Walker. 2014. Satisfiability-based Set Membership Filters. *Journal on Satisfiability, Boolean Modeling and Computation* 8 (01 2014), 129–148. <https://doi.org/10.3233/SAT190095>
- [50] S. Zbinden, A. Bärtschi, H. Djidjev, and S. Eidenbenz. 2020. Embedding Algorithms for Quantum Annealers with Chimera and Pegasus Connection Topologies. In *High Performance Computing*, P. Sadayappan, B. Chamberlain, G. Juckeland, and H. Ltaief (Eds.). Springer, 187–206.
- [51] Y. Zhou, J. Wang, and J. Yin. 2013. A Directional-Biased Tabu Search algorithm for Multi-Objective Unconstrained Binary Quadratic Programming Problem. *Proc. International Conference on Advanced Computational Intelligence (ICACI)* (2013), 281–286.